Post Access Report

Optimal Control of an Oscillating Surge Wave Energy Converter

Awardee: University of Washington

Awardee point of contact: Brian Polagye

Facility: NREL's Marine Renewable Energy Small Wave Tank

Facility point of contact: Rebecca Fao

Date: 3/7/2025

TEAMER
Testing & Expertise for Marine Energy

Executive Summary

During this project, we experimentally investigated the hydrodynamics and performance of a laboratory-scale oscillating surge wave energy converter (OSWEC). We initially had two project objectives: the first was to extract hydrodynamic parameters (added inertia, radiation damping, and excitation torque coefficients) of the device using forced oscillation and excitation tests, and the second was to build and test a data-driven model predictive controller that created a system model in real-time using data streams. However, due to experimental artifacts observed during initial testing, we shifted the focus of the second objective to instead characterize and compensate for these. Specifically, we looked at how flap buoyancy and driveline losses (primarily in the form of stiction) affected the dynamics and performance of the device. In addition, we assessed the influence of flap profile (rounded vs. square edges) on OSWEC hydrodynamics. Through this, we were able to develop a deeper understanding of OSWEC performance and provide guidance on strategies to counteract artifacts that may be present in laboratory models, but are absent in field-scale devices.

To do this, we tested a laboratory-scale OSWEC in the Sea Wave Environmental Lab (SWEL) wave tank at the National Renewable Energy Laboratory (NREL). We ran several types of experiments to investigate the hydrodynamics and performance of the device. The first set of experiments characterized flap buoyancy as a function of flap position by measuring the torque required to hold the flap at different angular positions. We used these results to isolate the hydrodynamic torque contribution from buoyancy in subsequent tests. We then ran forced oscillation tests, where we prescribed the flap to oscillate with a range of amplitudes and periods. From these tests, we extracted added inertia and radiation damping coefficients as a function of oscillation period and amplitude and compared the results to Boundary Element Method (BEM) simulations. Next, we locked the flap in its vertical orientation and exposed it to waves of different heights and periods. From these tests, we extracted excitation torque coefficients as a function of wave height and period that are also comparable to BEM simulation outputs. Finally, we performed control tests where we used the power train to emulate a PTO and extract power from the waves across different wave conditions. We used a linear damping control scheme and measured absorbed power as a function of damping coefficient for a range of wave and device parameters. Our main performance metric was capture width ratio (CWR). During these tests, we also investigated approaches to emulating a more buoyant flap and counteracting the effect of stiction in the driveline. This resulted in CWR curves as a function of damping coefficient for different wave conditions, flap buoyancies, flap profiles, and with and without stiction compensation.

We found that our experimental values of added inertia and radiation damping generally match the trends of BEM well, however there are regions where the two methods diverge. Experimental added inertia values were consistently less than BEM values for oscillation periods less than about 1.4 seconds, but showed good agreement for periods above 1.4 seconds. While further work is required to determine why this occurs, we hypothesize that this could either be caused by surface effects during the forced oscillation experiments or higher order hydrodynamics present in experimental forces. For radiation

damping, we found that experiments differed from BEM in two ways. First, the experimental radiation damping coefficients were often larger than those calculated from BEM, which is likely a consequence of viscous effects neglected in BEM. Second, there was discrepancy between BEM and experiments due to confinement effects, even when considering channel walls in simulation. However, when including channel walls, BEM and experiments agree well for excitation torque throughout the entire testing region. Overall, these results suggest that confinement can significantly affect hydrodynamic coefficients, with BEM capturing these effects with varying success. We also found that wave conditions, flap buoyancy, profile shape, and driveline stiction can significantly affect flap performance. In particular, we found that, despite the wider bandwidth of OSWECs relative to point absorbers, operating outside the optimal wave period significantly decreases power production and a more buoyant flap had significantly better performance.

Overall, even without a real-time controller, we achieved the overall goal of experimentally investigating the hydrodynamics and performance of this device. We discovered important and unexpected trends in performance, and collected time-resolved data to help us further investigate the underlying hydrodynamics responsible for these trends. In addition, we are currently using the time-resolved data from these experiments to build data-driven models of the dynamics, which can in turn be used to inform data-driven model predictive control of this device and address this objective in the future. Data collected for this work is available on the MHK DR under the title “Experimental Characterization of a Laboratory-Scaled Oscillating Surge Wave Energy Converter”.

1 Introduction to the project

Oscillating surge wave energy converters (OSWECs) are flap-type devices that harness power from ocean waves by utilizing the surge component of wave orbitals to generate oscillatory motion about a bottom hinge. These systems typically have complex hydrodynamics that make them difficult to understand, model, and control. Often, common modeling methods use the Cummins equation and Boundary Element Methods (BEM) to model time-resolved WEC behavior. However, these techniques are not always accurate, especially for energetic seas. In addition, many OSWEC systems use simple linear damping control schemes that may not fully optimize their behavior, especially in irregular waves. While there have been studies that expand the type of control applied to WECs to try to optimize performance, most of the studies focus on heaving point absorbers, and even fewer involve experimental testing. These issues leave a significant research gap into understanding the fundamentals of OSWEC dynamics, and how best to control the system to optimize power absorption and minimize loading.

During this project, we explored these research gaps experimentally by testing a laboratory-scaled OSWEC (developed by UW) at the Sea Wave Environmental Lab (SWEL) wave tank at the National Renewable Energy Lab (NREL) in Boulder, CO. With these experiments, we learned about the system in ways that can inform future design and control of the device. We had two main goals with this experimental campaign:

1. Our first goal was to **extract and analyze the frequency-dependent hydrodynamic coefficients that describe OSWEC behavior (added inertia, radiation damping, and excitation torque)** with two different flap profiles (round and square edges). We determined these coefficients experimentally under different loading conditions to learn more about the system dynamics. We are also planning to compare these results to a similar set of experiments conducted at UW where the device was under high confinement to understand how confinement affects system dynamics.
2. Initially, our second goal of this experimental campaign was to test a data-driven optimal control scheme and assess its benefits and costs on performance. We intended to build a data-driven model predictive controller (MPC) using dynamic mode decomposition to generate a linear system model in real time. This MPC would have been used to optimize power absorption while enforcing kinematic or dynamic constraints to promote structural integrity of the device. However, we were not able to achieve this objective because of several issues (see Section 7.2). Instead, during initial testing we observed two experimental artifacts that would need to be addressed for more advanced control strategies. Specifically, the flap dynamics were significantly affected by limited flap buoyancy and driveline stiction. Both of these are artifacts of a small-scale laboratory device, where sensor weight and parasitic losses are large relative to system mass and torques, respectively. For larger systems, we would expect these artifacts to play less of a role in system performance. Because of this, we shifted our focus to understanding how these artifacts affected system performance and how they could be compensated for in a scale-model experiment. Specifically, **we investigated how flap buoyancy, and stiction in the driveline affect flap performance and dynamics** under a linear damping control scheme. In addition, we evaluated performance for two flap profiles, to understand sensitivity to this

parameter. The results of these tests are being used to develop data-driven models of the OSWEC dynamics, which will help work towards our initial goal of building a data-driven model predictive controller for this system.

Data collected during this campaign is available on the MHK DR under the title "Experimental Characterization of a Laboratory-Scaled Oscillating Surge Wave Energy Converter".

2 Roles and Responsibilities of Project Participants

With this TEAMER funding, the UW team worked with NREL to run experiments in the wave tank at the Flatirons campus. NREL helped set up the experiments, operate the wave tank, and advise on analysis of the results. UW provided the OSWEC, the DAQ system, and a structure to adapt the current OSWEC test article to the dimensions of the NREL facility.

2.1 Applicant Responsibilities and Tasks Performed

UW's role in this project included the following:

- Adapting OSWEC test article for installation in the NREL tank. This included designing and building a base structure to account for a difference in operating water depth, developing procedures for lifting the OSWEC in and out of the tank fully assembled, and working with NREL to coordinate details on cable routing and electrical protection.
- Specifying wave conditions for tests.
- Shipping the OSWEC and DAQ system to NREL and assisting in commissioning the OSWEC in NREL's wave tank.
- Conducting on site testing with NREL supervision.
- Leading data analysis throughout testing to assure data quality and after testing to assess device performance.
- Uploading data to MHK-DR.
- Completing the Post-Access Report and Questionnaire.

2.2 Network Facility Responsibilities and Tasks Performed

NREL's role in this project included the following:

- Working with UW to specify modifications to the OSWEC test article for compatibility with NREL's facilities and Environmental Health & Safety requirements (e.g., water depth, electrical protection).
- Installing four calibrated wave probes in the wave tank, as well as assisting with connecting them to the applicant's DAQ.

- Installing and removing the OSWEC each week of testing to minimize the risk of water intrusion into the driveline.
- Running the wave tank under the conditions specified by the applicant and training applicant personnel on wave tank operation.
- Advising on data integrity during testing based on facility experience with similar systems.

3 Project Objectives

The assistance originally had two overall objectives: (1) characterize frequency-dependent OSWEC hydrodynamics under a variety of wave conditions and (2) experimentally test data-driven MPC schemes for a lab-scale OSWEC. However, after initial testing the second objective shifted to compensating for experimental artifacts including stiction on flap performance and hydrodynamics, as well as the sensitivity to flap profile.

The first objective involved extracting OSWEC hydrodynamic coefficients under different wave frequencies and amplitudes to assess how these testing parameters affect the hydrodynamic behavior. We also aimed to compare these results to those gathered previously at UW under high confinement (narrower wave basin) to understand the effects of confinement on system dynamics.

The second objective involved investigating the effect of flap shapes and experimental artifacts. Using the test article's power train, we aimed to develop methods to emulate additional flap buoyancy and offset the effect of driveline stiction. With these methods, we applied a linear damping control scheme and characterized flap performance, namely capture width ratio, as a function of linear damping coefficient. We aimed to compare performance between wave, flap, and driveline parameters.

During this experimental campaign, we aimed to investigate the following questions. First, for hydrodynamic characterization:

- How do the hydrodynamic parameters of the device change with wave frequency, amplitude, and flap profile?
- How do the results at NREL differ from comparable tests at UW? Are there any obvious effects from confinement?

Second, for investigating experimental artifacts:

- How do flap buoyancy, flap profile, and driveline stiction affect OSWEC performance?
- Can we counteract the effect of low flap buoyancy and driveline stiction using the OSWEC power train?

4 Test Facility, Equipment, Software, and Technical Expertise

We conducted experimental testing at the Sea Wave Environmental Lab (SWEL) at the Flatirons campus at NREL (Figure 1).

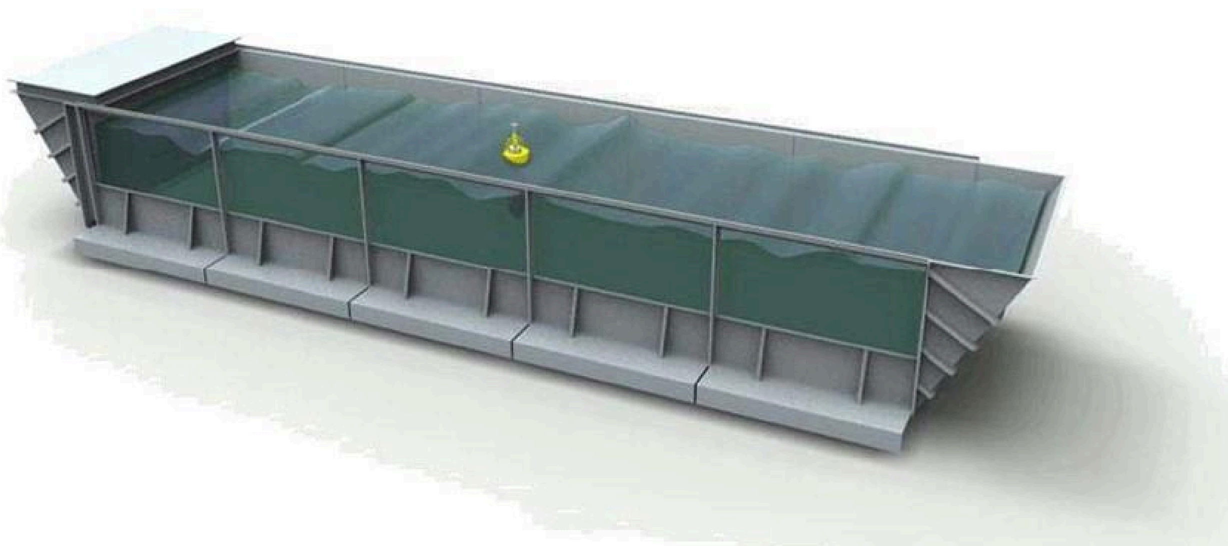

Figure 1: Rendering of the Sea Wave Environmental Lab (SWEL) wave tank at NREL with a representative point absorber wave energy converter.

This wave tank can be used for hydrodynamic testing of small-scale wave energy prototypes or other offshore systems where wave interactions are of interest (e.g., floating platforms). Combined with NREL's data acquisition and instrumentation capabilities, test articles can be rapidly tested and assessed.

The tank is 14 meters long, 2.5 meters wide, and operates at a constant water depth of 1.3 meters. Waves are generated by a flap-type, 2D wave actuator that can generate linear waves with amplitudes up to 125 mm and at a variety of periods (1 – 3 s). Waves are dissipated by a passive absorber at the far end of the flume. Wave height is measured by ultrasonic wave gauges (Section 6). One side of the flume is glass, which provides optical access for underwater observation. We installed and removed the fully-assembled test article with an overhead gantry crane.

5 Test or Analysis Article Description

These experiments used a laboratory-scaled oscillating surge wave energy converter (OSWEC), shown in Figure 2. OSWECs are flap-type wave energy converters that utilize the surge component of wave orbitals and flap buoyancy to create oscillatory motion about a fixed bottom hinge. This mechanical power can then be converted to electricity or used directly in a reverse-osmosis process for water desalination.

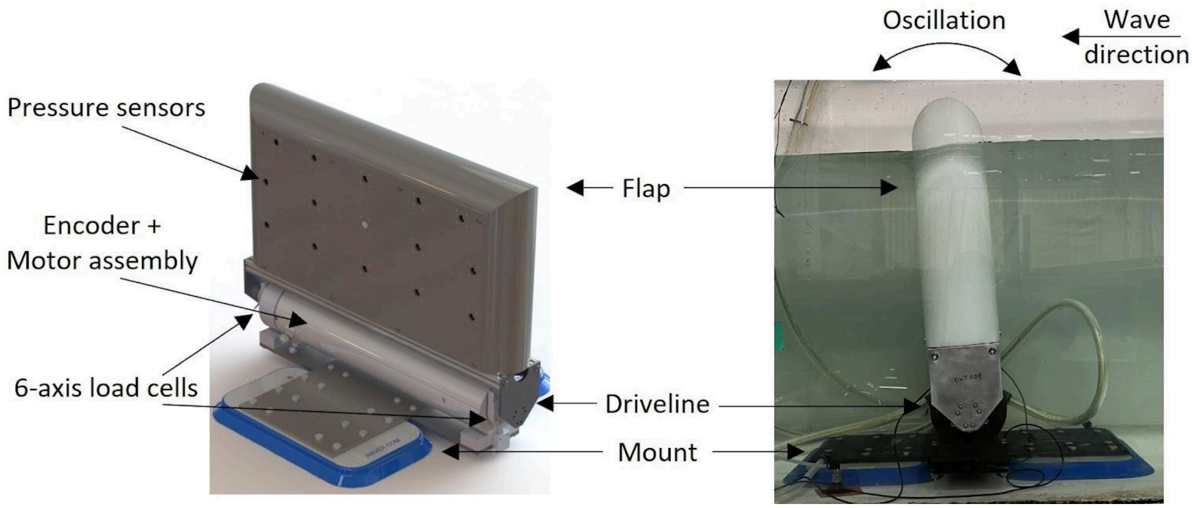

Figure 2: [Left] Annotated rendering of test article with included sensors. [Right] OSWEC test article installed in the wave tank at UW. Flap, driveline, and mount are highlighted in each image.

The system was composed of three components: the flap, driveline, and mount. The flap (0.85 m wide, 0.55 m tall, 0.1 m thick) was constructed of a low-density polyethylene case with an 80/20 aluminum frame filled with foam to produce buoyancy. There were two options for flap edge profile: rounded and square. The flap also contained an array of pressure sensors along the flap face and was connected to the driveline by two 6-axis load cells which measured the torques and forces imposed by the driveline and foundation, respectively. The powertrain consisted of a motor-gearbox assembly that could apply a variable control torque about the hinge to emulate a real power take-off (PTO). The powertrain was contained in a custom-made aluminum housing with a waterproof seal and bearing. There was also a leak sensor in the driveline housing that we used to detect any water that entered the vessel. The driveline was double-sided with one end of the shaft connected to the motor-gearbox (driven side) and the other secured by a sealed bearing (free side). Flap position was measured by an encoder on the gearbox output shaft and an encoder integrated with the motor. Further details of sensors are provided in Section 6. The OSWEC was secured to the wave tank base by a pair of vacuum plates. We ran all the experiments with the OSWEC connected to a base structure to raise the OSWEC in the water column, since the water depth could not be varied. With this frame, when the flap is vertical, it protruded from the water surface by about 10 cm.

Figure 3: CAD rendering of OSWEC with base frame and spreader bar assembly for lifting.

Further details of the OSWEC assembly are described in Table 1.

Table 1: Summary of system components.

Component	Size	Material	Mass	Function
Flap	Width: 85 cm Height: 45 cm Thickness: 14 cm	Outside: Low density polyethylene Inside: Foam, 80/20 Aluminum	25-27 kg	Interacted with waves to generate power. Attached to the driveline with two load cells to measure loading during testing.
Driveline	Length: 67.7 cm Diameter: 14 cm	Outside container: Machined aluminum	70 kg	Provided rotation axis for flap. Also included gearbox/motor assembly inside to emulate PTO.
Mount	Length: 72 cm Width: 72.5 cm Height: 3.25 cm	Aluminum	25 kg	Suctioned assembly to bottom of tank to keep test article fixed in place.
Base Frame	Length: 1.12 m Width: 1.02 m Height: 0.94 m	Steel and Aluminum	31 kg	Raised OSWEC in the water column so that the device was still surface-piercing. Also provided anchor spots for lifting the OSWEC in and out of the tank using the gantry crane.

6 Work Plan

6.1 Experimental Setup, Data Acquisition System, and Instrumentation

The OSWEC sensors included:

- An external encoder (Zettlex Midi Ultra IncOder) that measured flap position on the output shaft from the powertrain
- An encoder integrated into the motor (Parker MPP092) that measured its shaft position
- A pair of IP-68 rated 6-axis load cells (ATI Mini58) on either side of the driveline that measured torques and forces acting about the driveline
- 15 pressure sensors (Keller PR25Y) integrated into the face of the flap
- 4 ultrasonic wave gauges (ToughSonic 14) that measured wave elevation upstream of the flap on a lateral offset

These sensors were connected to a National Instruments DAQ (PCI-6255) that was controlled by MATLAB Simulink. All signals were acquired at 1000 Hz, though the ultrasonic wave gauges updated at a slower rate. Further details for each sensor are provided in Table 2. Details on the DAQ we used for the experiments are provided in the Appendix.

Table 2: Sensor details, including range, accuracy, and calibration date.

Sensor	Range	Accuracy	Calibration
Force/torque sensor (driven side) (Mini58, ATI Industrial Automation) (digital, voltage)	F_x: 1400 N F_y: 1400 N F_z: 3400 N M_x: 60 N-m M_y: 60 N-m M_z: 60 N-m	F_x: 1% of full-scale F_y: 1% of full-scale F_z: 1% of full-scale M_x: 1.75% of full-scale M_y: 1.75% of full-scale M_z: 1.75% of full-scale	Mfg. calibration 2021
Force/torque sensor (free side) (Mini58, ATI Industrial Automation) (digital, voltage)	F_x: 1400 N F_y: 1400 N F_z: 3400 N M_x: 60 N-m M_y: 60 N-m M_z: 60 N-m	F_x: 1% of full-scale F_y: 1% of full-scale F_z: 1% of full-scale M_x: 1.75% of full-scale M_y: 1.75% of full-scale M_z: 1.75% of full-scale	Mfg. calibration 2023
Encoder (Zettlex Midi Ultra IncOder)	N/A	19-bits	Mfg. calibration 2021
Pressure sensor (Keller PR25Y) (analog, current)	0 - 10 kPa gauge	+/- 0.5% of full-scale	Mfg. calibration 2022
Ultrasonic wave gauges (Senix ToughSonic 14) (analog, voltage)	0.102 - 3.0 m (range from transducer)	3279 steps of 0-20 mA (scaled between user-set end points)	March 28th 2023

Installation: At the start of each day of experiments, if the OSWEC was not already installed in the tank, we installed the OSWEC system near the center of the SWEL tank using the gantry crane. In addition to the primary vacuum plates that secure the OSWEC to the tank, individual hand-pumped suction plates were used to secure cable bundles to the side of the tank near the waterline.

Testing: We ran an initial test at the start of each set of experiments where we centered the flap to its neutral vertical position and acquired load cell data for one minute as a tare value. This tare was repeated at least every hour during testing to minimize the effects of sensor drift on experimental results.

Following the initial tare, we often performed free decay tests, where we commanded the controller to apply a positive or negative torque about the hinge to rotate the flap to an equilibrium position, then released the torque to allow the flap to return to its neutral position. Across days, by comparing the tare-corrected force and torque time series for each load cell, as well as flap position over time, we could identify anomalous load cell performance or changes to the mechanical properties of the flap. These tests ensured the control system was behaving as we expected and the dynamics were repeatable.

After these initial tests, we ran the experiments outlined in Section 6.3. We allowed 8-9 minutes between tests to allow the tank to settle and to visualize data from the previous test.

Data Processing: After each test, we plotted the encoder position data, as well as forces and torques for both load cells. We considered both the raw and tare corrected values. This allowed us to identify any unexpected patterns in the data to catch issues early and avoid large losses in data collection. We also verified that each test fell within the calibrated range for the load cells and was not overloading the motor.

Removal: At the end of the week, we removed the OSWEC from the water using the same harness and crane procedure as the installation. This was to minimize the risk of leaks in the driveline housing or load cells due to long-term submergence in water. The wave gauges stayed installed throughout the experimental campaign. All data was locally and uploaded to a Google Drive account every day that was shared between UW and NREL.

6.2 Numerical Model Description

We used WAMIT [1] to simulate hydrodynamic coefficients and compared these against experimental values of added inertia, radiation damping, and excitation torque. The simulations included the flap and driveline, but not the base structure. However, because the structure is low in the water column relative to wave orbital decay, we expect this simplification to have limited effects on the BEM results. We ran simulations with both a round and square flap and considered results with and without channel walls of the same width of the SWEL wave tank.

6.3 Test and Analysis Matrix and Schedule

The first set of tests was performed without the OSWEC installed to ensure the wavemaker was generating the wave elevation we were commanding and assess the degree of reflections we should expect. For these tests, we installed the wave gauges along the length of the tank, commanded the wavemaker to produce the desired wave condition, and compared the output of the wave gauges to what we would expect based on our command. We ran these tests using two different wave types (Table 3):

- **Regular waves**: Four wave periods (1, 1.5, 2, and 3 s) and five wave heights (25, 50, 75, 100 and 150 mm)

- **Irregular waves:** Pierson-Moskovitz spectrum with three significant wave heights (50, 75, and 100 mm) and two peak periods (1.5, and 2 s).

All of these wave conditions were also used in experiments with the OSWEC.

Table 3: Summary of tests in empty basin used to evaluate the wavemaker's ability to generate the desired wave elevation.

Wave type	Measured parameter	Wave periods [s]	Wave heights [mm]	Total tests
Regular	Wave elevation	1-3	25-125	24
Irregular (P-M spectrum)	Wave elevation	1.5-2	50-100	8

After characterizing the wavemaker, there were two main categories of testing: hydrodynamic characterization and control tests. Summaries of the hydrodynamic characterization and control tests are shown in Table 4 and Table 5, respectively. We allocated about 10 minutes for each test, which includes 1-2 minutes of run time and 8-9 minutes for the water to settle between tests. With this timeline, we could reasonably run at least 20 tests in one day, allowing ample time for installation, removal, and real-time data analysis to ensure data quality.

The hydrodynamic testing determined the frequency-dependent hydrodynamic coefficients of the device, including excitation torque, radiation damping, and added inertia. The first set of experiments measured excitation torque by locking the flap in its neutral vertical position and generating regular waves with different periods and amplitudes to measure the loading on the device. The range of wave periods we tested ranged from one to three seconds at an increment of 0.25 seconds, resulting in a total of 11 frequencies for each wave height, with some tests being limited by the capabilities of the wavemaker. We tested four different wave amplitudes: 25, 50, 75, and 100 mm. This resulted in a total of 42 tests run (with some repeated tests and some tests excluded due to wavemaker limitations), which took about two days.

The next set of tests were forced oscillation tests where we prescribed the flap to oscillate with a certain amplitude and period and extract added inertia and radiation damping coefficients. Each set of forced oscillation tests were run with two different flap profiles, one with round edges and one with square. We tested the same 11 oscillation periods as the excitation experiments and tested three oscillation amplitudes: 2.5, 5, and 10 degrees. This resulted in 78 planned tests, however we ran a total of 104 forced oscillation tests over about six days, which included several repeat tests to verify results. Details on how we extracted added inertia and radiation damping from the data is given in Section 6.6.3.

Table 4: Summary of hydrodynamic characterization tests.

Test	Measured parameter	Wave / Oscillation periods [s]	Wave heights or Oscillation amplitudes	Flap(s)	Total tests
Excitation	Excitation torque coefficient	1-3	25-100 mm	Round	42
Forced oscillation	Radiation damping and added inertia	1-3	2.5-10 deg	Round and Square	104

The third category of tests we completed are control tests, of which there were two main rounds. The first round investigated the effect of wave properties on flap performance, and the second investigated the effect of flap buoyancy, flap shape, and driveline stiction on flap performance. All of these tests were run with a linear damping control scheme, and we tested a range of damping coefficients to identify the peak performance (details in Section 6.6.3). We refer to a group of tests with the same conditions but varying damping coefficients as a “PTO damping sweep”. From each sweep, the goal was to generate a performance curve of capture width ratio as a function of the damping coefficient. For the first round of control tests, we tested three wave periods (1, 1.5, and 2 s) at two different wave heights (50 and 100 mm) with an additional set of tests with a wave period of 1.5 seconds and a height of 125 mm. Each wave condition was tested with 11 damping coefficients ranging from 0 to 100 Nms, except for the case of a wave height of 125 mm where we were limited by the motor and load cell torque limit to only test up to 50 Nms. The wave and control parameters were determined from tests previously run at UW and based on motor and sensor limits. This resulted in 72 tests total and the tests are summarized in Table 5.

Table 5: Summary of the first round of control tests.

Wave height [mm]	Wave period [s]	B_{PTO} [Nms]	Flap(s)	Total tests
50	1	0 - 100	Round	11
50	1.5	0 - 100	Round	11
50	2	0 - 100	Round	11
100	1	0 - 100	Round	11
100	1.5	0 - 100	Round	11
100	2	0 - 100	Round	11
125	1.5	0 - 50	Round	6

For the second round, we ran seven PTO damping sweeps, all with the same wave height of 100 mm and period of 1.5 s (determined to be the best performing wave condition from the first round). The tests are summarized in Table 6. We ran four sweeps to characterize the effect of flap buoyancy on performance. To do this, we used the motor to apply both the linear damping control torque and an additional torque that followed the buoyancy torque profile determined from the buoyancy tests. The emulated buoyancy was 5, 7.5, and 10 times the baseline flap buoyancy. This, together with repeating the sweep with no added buoyancy torque, resulted in a total of 44 tests. Next, we ran two PTO sweeps that, in addition to the linear damping control and added buoyancy, also applied a variable torque that aimed to offset the effect of stiction in the system. To quantify the effect of the stiction, we read in the torque measured by the load cell on the free end of the driveline (this cell only measures the torque losses from the seals and bearing packs in the driveline), and assumed that the losses were symmetrical on both sides. Consequently, we used the motor to apply twice that measured torque in the opposite direction of the losses to account for stiction on both the driven and free end of the driveline. Based on initial tests, we added an empirical correction to further compensate for the difference in losses between the driven and free end of the driveline. Using this correction, we ran a PTO damping sweep with no additional buoyancy added, and ran a PTO damping sweep where we applied 10 times the nominal buoyancy. This resulted in a total of 22 tests.

For the final two PTO sweeps, we removed the round edges of the flap and replaced them with square edges to explore how flap profile affected device performance. We ran two PTO sweeps, one with no added buoyancy torque and one where we applied 10 times the nominal buoyancy. This resulted in a total of 25 tests (with three repeated tests).

Table 6: Summary of the second round of control tests. All tests were conducted with a wave height of 100 mm and wave period of 1.5 seconds.

Buoyancy Added [x100% original buoyancy]	Stiction Correction	B_{PTO} [Nms]	Flap(s)	Total tests
0	No	0 - 100	Round and Square	25
5	No	0 - 100	Round	11
7.5	No	0 - 100	Round	11
10	No	0 - 100	Round and Square	22
0	Yes	0 - 100	Round	11
10	Yes	0 - 100	Round	11

While we initially planned for these tests to be conducted over the course of five weeks, we tested for a total of ten weeks, with a break of about 4.5 months in between. This allowed us to analyze the data in detail and refine the testing matrix based on the first round of results. In addition, a number of shakedown tests were performed to identify a routing for the pressure sensor cables that would minimize the amount of force they applied to the test article.

6.4 Safety

All NREL required safety practices and procedures were followed as laid out in the NREL Flatirons Campus General Safe Operating Procedure (SOP) and the Wave Tank Operations Work Safe Activity. An additional Safe Work Permit (SWP) was developed to cover aspects of the project not covered under these existing work authorization documents. All NREL staff and UW visitors complied with the SOP and job walk while working at the Flatirons Campus (FC). UW visitors participated in an NREL Environmental Health & Safety orientation before they were allowed to participate in testing activities at the FC.

Specific safety policies and procedures relevant to this project that were followed include:

- Only authorized personnel operated the wave tank and crane
- Hard hats were worn when crane operations were in progress
- Safety glasses were worn in the facility at all times
- Working alone around the wave tank was not permitted
- Life vests were worn when working over or inside the wave tank

Additionally, a thorough electrical safety inspection was conducted on the test article prior to beginning work. UW and NREL worked closely together to ensure that all aspects of the test article were able to satisfy NREL safety protocols (see further discussion in Section 7.2).

6.5 Contingency Plans

The following contingency plans were potentially relevant to project execution:

1. *Suction plates unable to restrain OSWEC motion*: This could occur if the suction plates were unable to form as strong a seal in the NREL flume as they do at UW. If this occurred, the experimental matrix could be truncated to reduce loading, the plates could be reinforced with magnetic clamps (the strongback element in the suction plates is ferrous steel), or control experiments could be run with the flap mounted directly to the bottom of the wave basin, reducing excitation forcing. In practice, none of these contingencies were required.
2. *Damage to one of the load cells*: UW had experienced problems with one of the original system load cells involving a steady "drift" on one channel. This is typically associated with mechanical overload, but during prior testing, forces were well within manufacturer specifications. To mitigate this concern, a backup load cell was procured. In practice, neither load cell experienced any anomalies.
3. *Wave reflections contaminate hydrodynamic characterization experiments*: The passive wave absorber in the NREL wave tank does not perfectly dissipate incident waves. Similarly, reflections and radiated waves from the OSWEC flap can reflect off the wave maker. Consequently, after some time, reflected waves begin to influence the OSWEC dynamics. This can be characterized by assessing the incident wave field and variation in hydrodynamic coefficients over time. Mitigation measures include reducing the duration of each test or excluding test conditions where wave reflections are significant. In practice, experimental duration was truncated to minimize the influence of reflections.

There were some contingencies that could not be entirely mitigated against. This included loss of driveline seal integrity, which would damage the gearbox and motor. Because it would be infeasible to have a spare driveline available, mitigation measures were employed, including a leak sensor and removing the test article from the water after each week of testing.

6.6 Data Management, Processing, and Analysis

6.6.1 Data Management

Data was collected and stored on a local computer owned by UW. We also used a Google Drive folder that both UW and NREL could access to backup raw and processed data files along with the metadata. Finally, UW used a Git repository to manage processing scripts for tests and shared the repository with NREL prior to experiments and analysis.

We uploaded all data from the experiments that are needed to reproduce the results of this project and are relevant to the marine energy community. Table 6 summarizes the uploaded data to the MHK DR.

Table 6: Summary of which data will be uploaded to MHK DR.

Data description	Format	MHK DR
Metadata/configuration file	MAT-file	Yes
Raw time series	MAT-file	Yes
Processed time series data (load cell and encoder data)	MAT-file	Yes
Hydrodynamic parameters (added inertia, radiation damping, and excitation torque)	MAT-file	Yes
Processed performance data (absorbed power time series, OSWEC capture width ratio)	MAT-file	Yes
Description of variables	Text file	Yes

6.6.2 Data Processing

Data from the load cell, encoder, and pressure sensors were saved to a folder on the local computer for every test. For each set of tests, the parameters of the system and controller were saved so they could be referenced during post-processing. The data was then processed to remove sensor noise (low-pass filter), calculate angular velocity and acceleration by differentiation, and transform the load cell measurements to a global, tare-corrected reference frame (Figure 7).

We incorporated multiple checks during testing to assure data quality during testing. First, as previously discussed, at the beginning of each testing day, the free-decay tests ensured that all sensors and mechanical components were operating as expected. Second, tare data were collected hourly to identify and track any drift in the load cell measurements throughout the testing. Third, we plotted encoder position and load cell values for both load cells after every test to evaluate data quality and ensure the system was acting as we expect. Lastly, we periodically dedicated time to data analysis throughout the days and weeks of testing to identify any issues with collected data and adjusted the testing matrix accordingly.

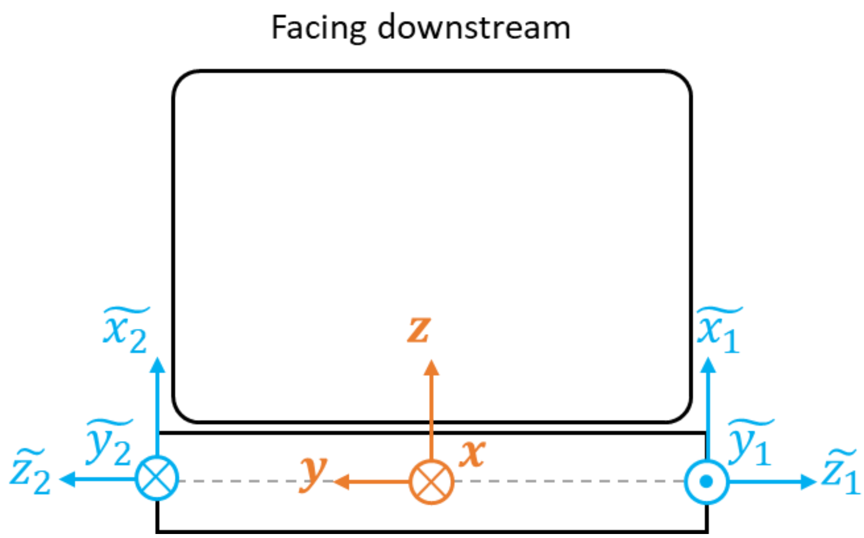

Figure 7: Diagram of OSWEC showing local coordinate systems for each load cell (blue, labeled 1 and 2), and the global coordinate system (orange). Circles with crosses represent vectors facing into the page, while circles with dots in the center represent vectors facing out of the page. The direction into the page points downstream, in the direction of wave propagation.

6.6.3 Data Analysis

Hydrodynamic characterization: The computed variables for the hydrodynamic characterization tests include excitation torque coefficient (τ_e), (extracted from the locked flap experiments), added inertia (I_a), and radiation damping (B_r) (extracted from the forced oscillation tests). To calculate these parameters, we first isolated the hydrodynamic torque, τ_h, from the measured torque from the load cells, τ_m, as described in [2]:

$$\tau_h = \tau_m - \tau_i - \tau_b - \tau_w,$$

where τ_i, τ_b, and τ_w are the torque due to inertia, buoyancy, and weight of the flap, respectively, all of which have been characterized for this flap from previous experiments. The model for buoyancy torque was confirmed through the buoyancy tests run at NREL. The measured torque corresponds to τ_y on each load cell in the global coordinate frame.

The excitation torque coefficient is the Fourier coefficient of the hydrodynamic torque from the locked flap experiments, $\widehat{\tau_h}(\omega)$, divided by the nominal wave amplitude, A, as follows:

$$\tau_e(\omega) = \frac{\hat{\tau}_h(\omega)}{A},$$

where ω is the incident wave frequency. For this analysis, we use the FFT function in MATLAB to obtain the $\widehat{\tau_h}$ at the incident wave frequency.

For the forced oscillation tests, we extract both the radiation damping coefficient, B_r, and added inertia, I_a, assuming that these forces can be decomposed through a Morrison relation as:

$$\tau_h = - B_r\dot{\theta} - I_a\ddot{\theta},$$

where $\dot{\theta}$, $\ddot{\theta}$ are the angular velocity and acceleration of the flap, respectively. To determine these coefficients, we extract the Fourier coefficients of the hydrodynamic torque ($\hat{\tau}_h$) and rotational position ($\hat{\theta}$) at the wave frequency. Under the assumption of periodic motion (prescribed by the motor), $\hat{\dot{\theta}} = i\omega\hat{\theta}$ and $\hat{\ddot{\theta}} = - \omega^2\hat{\theta}$, such that we obtain:

$$\hat{\tau}_h(\omega) = (- i\omega B_r + \omega^2 I_a)\, \hat{\theta}(\omega).$$

Now, we can define $Y = \frac{\hat{\tau}_h}{\hat{\theta}}$, and solve for B_r and I_a:

$$I_a(\omega) = \frac{Re(Y)}{\omega^2}, \qquad B_r(\omega) = \frac{Im(Y)}{-\omega}.$$

We ran this procedure for each oscillation and wave frequency to characterize the frequency dependence for each hydrodynamic parameter. For each test, we also performed a moving window analysis to determine how these coefficients shift throughout the time of the test to identify potentially problematic wave reflections (Section 6.5).

Control: For the control experiments, to assess the performance of each control scheme, we calculated the absorbed power, P_a, as:

$$P_a = \tau_{PTO}\dot{\theta},$$

where τ_{PTO} is the torque applied to the flap by the driveline (i.e., emulated PTO), including the losses from the seals and bearings. We measured τ_{PTO} as the sum of the moments measured by both load cells in the global reference frame. For the linear damping control scheme (without considering added buoyancy or stiction correction), the PTO torque is:

$$\tau_{PTO} = B_{PTO}\dot{\theta} + \tau_{losses},$$

where B_{PTO} is the nominal PTO damping coefficient that we input to the controller, and τ_{losses} is the torque due to the losses from seals and bearings from the system. These losses are primarily due to stiction and act in phase with velocity. To account for these losses, we use an effective damping coefficient, $B_{PTO,eff}$, such that:

$$\tau_{PTO} = B_{PTO,eff}\dot{\theta},$$

where we find $B_{PTO,eff}$ using linear regression to find the value that minimizes the two-norm error between τ_{PTO} and $B_{PTO,eff}\dot{\theta}$. Using $B_{PTO,eff}$ ensures we are consistent when comparing different tests and accounting for the “losses” acting on the flap. During regular wave experiments, we stepped through B_{PTO} values to identify the performance of the flap as a function of damping coefficient and identify the optimal PTO damping coefficient for each wave condition.

Once we have the absorbed power for the different control schemes, we calculate the capture width ratio of the OSWEC, CWR, by normalizing the time-average absorbed power, $< P_a >$, by the average wave energy flux per unit crest length, P_w, and the width of the OSWEC, w:

$$CWR = \frac{<P_a>}{wP_w}.$$

The average wave energy flux contained in a regular wave over one wavelength is described as:

$$P_w = \frac{1}{2}\rho g A^2 c_g,$$

where ρ is the water density, g is gravitational constant, and c_g is the group velocity, described as:

$$c_g = \frac{1}{2}\sqrt{\frac{g}{k}tanh(kh)},$$

where k is the wavenumber of the incident wave and h is the water depth.

7 Project Outcomes

7.1 Results

Buoyancy Tests: Figure 8 summarizes the results of the buoyancy tests for the round and square flaps. We found that the restoring torque is a cubic function of flap position for both flaps, therefore we were able to fit a cubic polynomial function to the curves, obtaining an analytical expression for restoring torque as a function of position. For the round flap, we found that between +/- 15 degrees the restoring torque is mostly linear, but small in magnitude. Since the flap operates in this region for many tests, these plots give insight into how little the baseline buoyancy affects flap dynamics. For the square flap, we found that the restoring torque to be even smaller in the linear region and were unable to fit a single cubic function to the entire range of data for the square flap. As a result, we focused the fit on the data from +/- 28 degrees and adjusted the coefficients slightly to ensure that the fit is monotonic with respect to flap position. This resulted in a less accurate fit near the edges of the position region, however the flap rarely reaches this region in normal operation, so we expect the discrepancy to have little effect on subsequent hydrodynamic analysis. The fits developed with these tests are used for isolating the hydrodynamic torque in the forced oscillation tests (see Section 6.6.3) and for emulating buoyancy in the control tests.

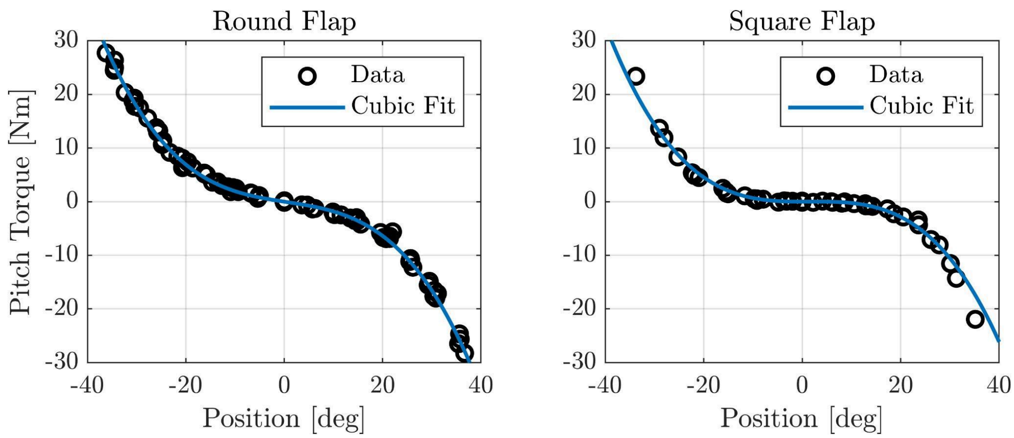

Figure 8: Restoring pitch torque as a function of flap position for the round (left) and square (right) flap. The blue line shows a cubic fit to the experimental data (black dots).

The relatively limited buoyancy is a consequence of design decisions for the OSWEC. First, the edge material is relatively dense and was chosen for its machinability and rigidity, not buoyancy. Second, while the foam internal to the flap provides buoyancy, the space required for the array of pressure sensors and their cabling reduced the volume available for foam. An alternative flap design with a greater internal volume (e.g., a tapered wedge) could be beneficial, but would complicate the design of edge profiles.

Excitation Tests: Results of the excitation experiments for the round flap, as compared to BEM simulations, are shown in Figure 9. We extracted excitation torque coefficients using the torque measured by the load cells during the locked flap tests and normalizing the magnitude by the nominal wave height (Section 6.6.3). Experiments and BEM agree well, especially when including channel walls in the BEM simulation. BEM results with and without a channel wall disagree between 1.2 and 1.3 second periods, corresponding to wavelengths between 2.3 and 2.6 meters. At these wave periods, the wavelength is about equal to the channel width of 2.5 meters, so any wave component in the cross-flume direction (caused by diffraction and/or radiation) is close to resonance and could significantly affect the results. We observe cross-channel wave action in experiments (Figure 14) and the experimental results agree with BEM with channel walls in this region. This suggests confinement can play a significant role in excitation torque coefficients, especially when operating at frequencies close to the resonant frequency of the cross-channel, and should be considered for BEM modeling of experiments, even when test article size is about ⅓ of the channel width. Finally, while the experimental values show some amplitude dependance, which is indicative of nonlinearity, there is not a consistent trend.

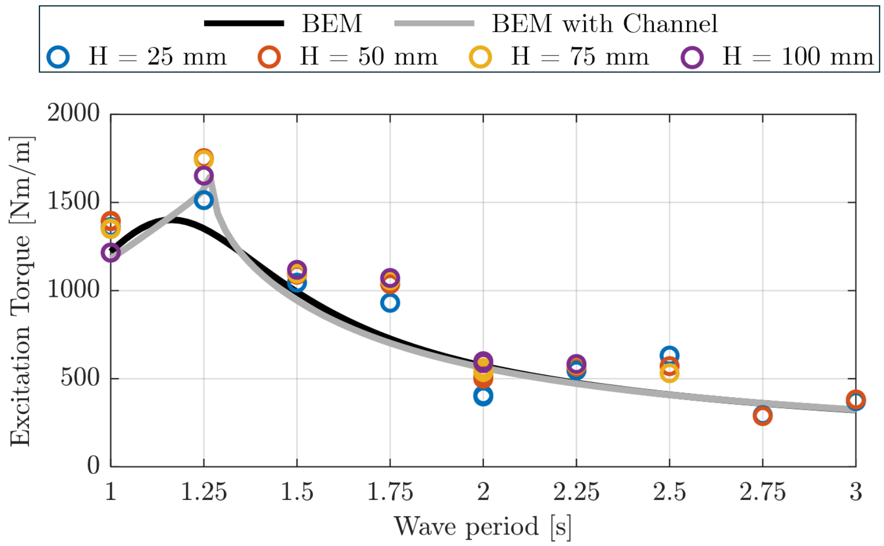

Figure 9: Excitation torque coefficient as a function of wave period. Solid lines represent BEM results with (gray) and without (black) the channel walls. Markers represent experimental values from locked flap tests with color corresponding to incident wave height during the test.

Forced Oscillation Tests: A summary of the hydrodynamic coefficients extracted from the forced oscillation tests using the round and square flap are shown in Figure 10. We extracted both added inertia and radiation damping coefficients from the torque, velocity, and acceleration data from the forced oscillation tests (Section 6.6.3). In general, both the experimental added inertia and radiation damping coefficients follow the same general trend as the BEM results, with some interesting discrepancies. First, including a channel in the BEM simulation did not improve agreement with experiments for either flap. Unlike the excitation torque coefficient, the experimental results for added inertia do not show significant confinement effects between 1.2 and 1.3 second periods. For both flaps, the experimental added inertia coefficients are consistently less than the BEM added inertia coefficients for periods less than ~1.4 seconds and turn negative for periods below 1.25 seconds. This result could be physical, as surface effects can produce negative added mass/inertia when the potential energy of the fluid flow from WEC motion outweighs its kinetic energy [3]. However, this also could be due to error in fitting the signals to a single frequency sine wave that neglects the presence of higher-order dynamics. We plan to look into this disagreement further in future work.

For the radiation damping coefficient, there are some interesting differences between the results for the round and square flaps. For the round flap, experimental results match the trend of BEM results well, however there is appreciable spread in the data points, especially at T = 1.5 seconds, making it difficult to draw definitive conclusions. Including a channel in the BEM simulation improves agreement for periods around 1.25 seconds, but there is still substantial disagreement. For the square flap, there is more significant disagreement between BEM and experiments, especially around the cross-channel resonant period of 1.25 seconds where experiments show a peak not reflected in BEM. This suggests that confinement is affecting results in a way that is not captured by BEM, even when channel walls are included in the simulation. In addition, the experimental radiation damping is consistently higher than predicted by BEM models, which we expect is due to viscous losses that are not represented by potential flow and therefore not captured by BEM. Although this trend is also seen for the round flap, it is more prominent with the square flap results, which is consistent with elevated viscous losses from the sharp edges. These results highlight some limitations of BEM, including not capturing confinement or viscous effects, and demonstrates the importance of using experimental data to validate linear potential flow models.

For both flaps, neither added inertia or radiation damping show significant dependence on oscillation amplitude, suggesting that we were operating in a mostly linear regime where there is little-to-no amplitude dependance. Because of this, the disagreement between experiments and BEM is particularly interesting.

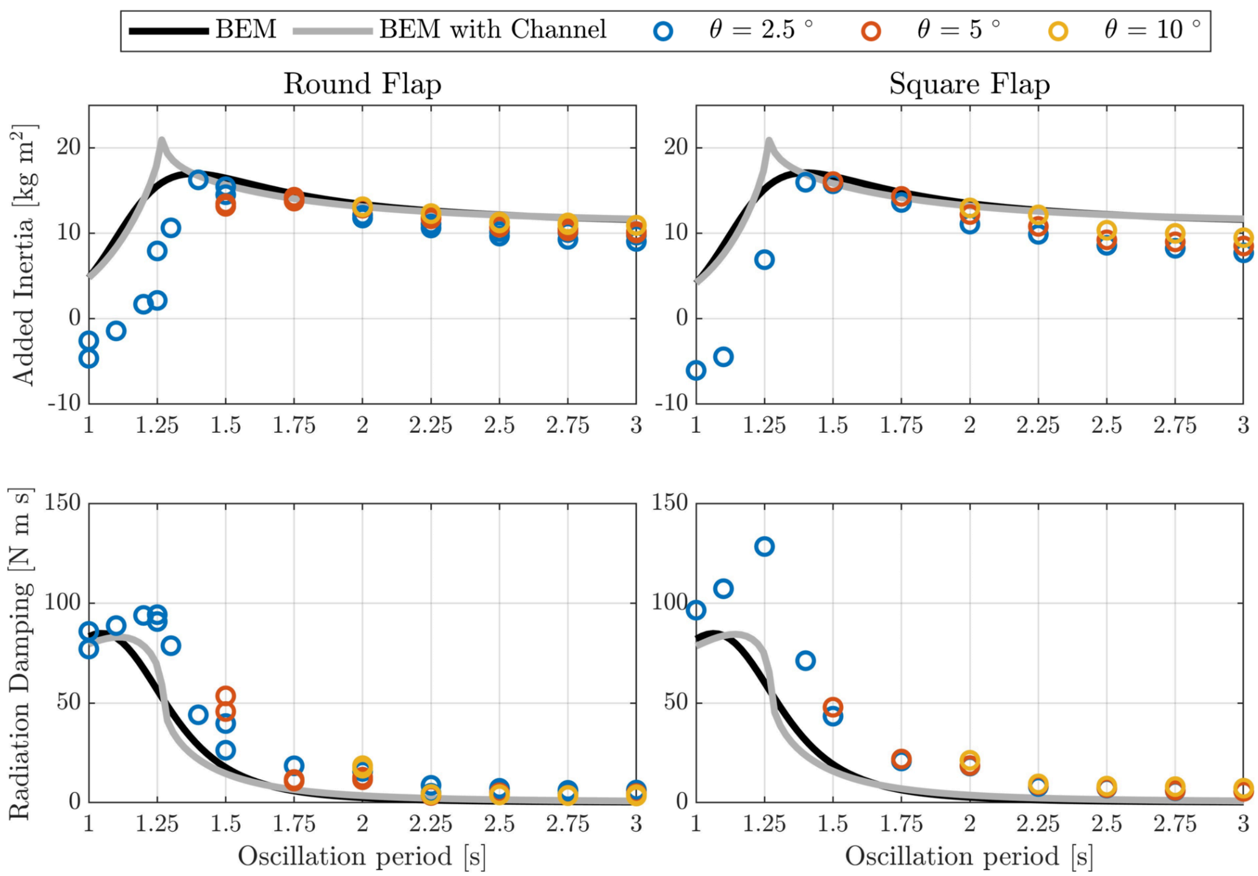

Figure 10: Added inertia coefficients (top row) and radiation damping coefficients (bottom row) as a function of oscillation period for the round flap (left column) and square flap (right column). Experimental results are represented by circles where color represents different oscillation amplitudes with blue as 2.5 degrees, orange as 5 degrees, and yellow as 10 degrees. Gray and black lines represent BEM output for the flap with and without a channel, respectively.

Control Tests: Figures 11 and 12 summarize the results of the control tests. Figure 11 shows the capture width ratio (CWR) as a function of effective damping coefficient for different wave conditions. We found overall that the efficiency of the device is low (CWR of less than 0.1). A wave period of 1.5 seconds results in the highest efficiency, while a wave period of 2 seconds has the lowest efficiency. Further, CWR depends on wave height, with a height of 100 mm resulting in the highest efficiency. Interestingly, a wave height of 125 mm results in lower efficiency. Overall, these tests helped us understand how the performance of our device is affected by wave conditions, and we used this data to inform conditions for tests investigating how to address the experimental artifacts of low flap buoyancy and stiction losses.

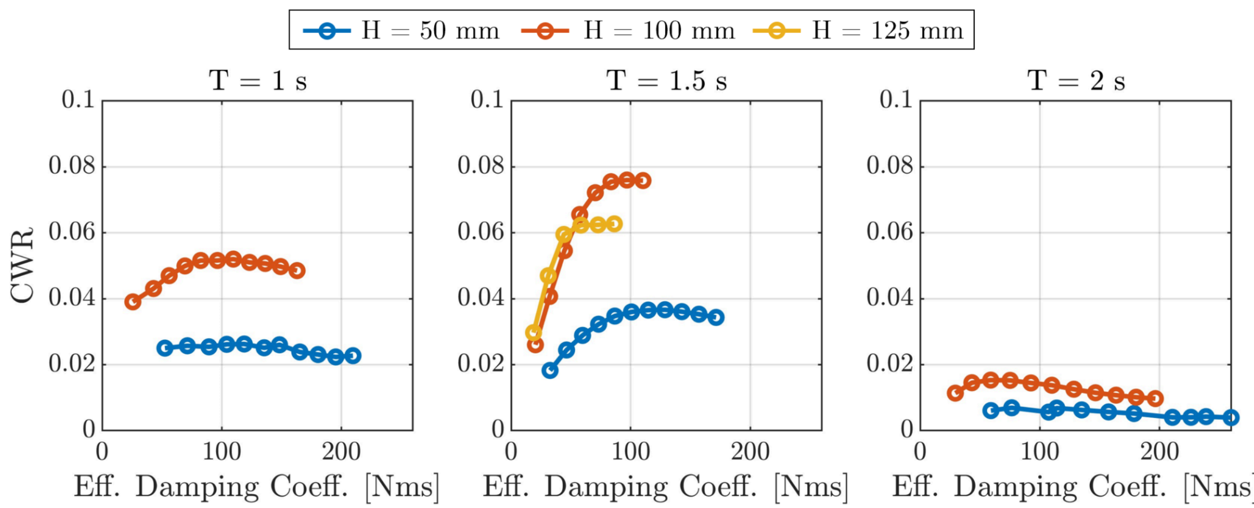

Figure 11: Capture width ratio as a function of effective damping coefficient for different wave conditions. Each panel represents a wave period with the left showing a period of 1 s, the middle showing a wave period of 1.5 s, and the right showing a period of 2 s. Color represents the wave height with blue as a 50 mm wave height, orange as a 100 mm wave height, and yellow as a 125 mm wave height.

Figure 12 summarizes the results of the second group of control tests where we explored how changes to flap buoyancy, flap edges, and reducing stiction affect performance. The first set of data shows CWR as a function of effective damping coefficient when emulating different amounts of buoyancy based on the fit for restoring torque from the buoyancy tests. Results show that increasing the buoyancy of the flap improves the CWR of the device for all added buoyancy and damping coefficients. In addition, the maximum CWR occurs at lower effective damping coefficients when buoyancy increases and the benefit of added buoyancy appears to decrease as effective damping coefficient increases. This is consistent with theory. Specifically, by increasing the hydrodynamic stiffness through emulated buoyancy, we are changing the resonant period of the flap to be closer to the wave period, allowing greater power absorption. At the same time, increasing damping reduces the influence of hydrodynamic stiffness in device performance. The second set of data shows how CWR is affected by flap profile (i.e., round versus square edges). In general, we were not able to fully resolve the CWR curves for the square flap because we were limited by the calibrated range of the load cells. Therefore, we were not able to confirm the peak CWR for the square flap, but it is clear for both buoyancies that the maximum CWR occurs at a larger effective damping coefficient for the square edges relative to the round edges. However, for lower effective damping coefficients (i.e., less than 60 Nms), the flap profile has little effect on CWR, and emulated buoyancy has little effect for the square flap in this region. The latter may be a consequence of elevated viscous damping counteracting power absorption, but requires further exploration to confirm. The final set of data explores the effect of applying a stiction correction to the flap. We found that, as expected, the stiction compensation extends the CWR curve to lower effective damping values. However, because stiction is largely in phase with velocity, the correction does not fundamentally alter performance for a given effective damping coefficient. With these results, we are confident we are reducing the effect of stiction in our system and enabling the use of a broader set of control strategies. Going forward, we also plan to investigate how this compensation affects time-resolved dynamics.

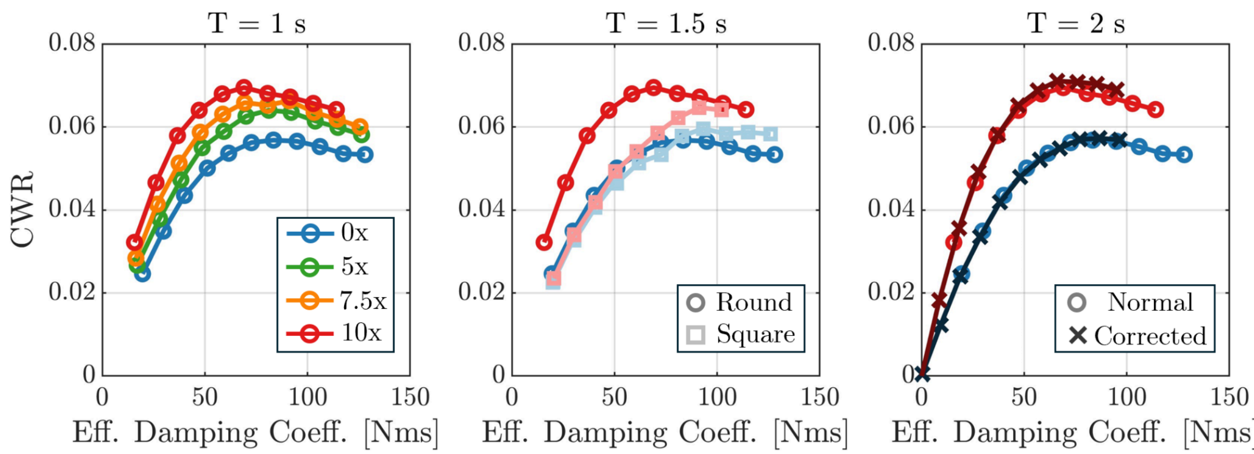

Figure 12: [Left] Capture width ratio as a function of effective damping coefficient for different amounts of emulated buoyancy for the round flap with no stiction correction applied. The amount of buoyancy added ranges from 0 (blue), 5 (green), 7.5 (yellow), and 10 (red) times the nominal buoyancy of the flap. Dashed lines represent the effective damping coefficient corresponding to the maximum CWR for zero (blue) and 10 (red) times added buoyancy. [Center] CWR as a function of effective damping coefficient for the round flap (circles) and square flap (squares) with no stiction correction applied. Blue lines represent no buoyancy added while red lines represent 10 times the nominal buoyancy of the flap added to the system. [Right] CWR as a function of effective damping coefficient for the round profile with no correction (circles) and a stiction correction applied (crosses). Blue lines represent no buoyancy added while red lines represent 10 times the nominal buoyancy of the flap added to the system.

Experimental Phenomena: As a result of this testing, we identified interesting experimental phenomena that we did not previously account for and had significant effects on flap dynamics and performance. First, because of the limited baseline buoyancy, we found that the flap oscillations tended to drift in the direction of wave propagation. Instead of oscillating about its neutral vertical position, the position the flap would oscillate about would change throughout the test, such that the flap would be tilted further in the direction of wave propagation as the test went on. This drift in mean flap position would sometimes cause the wave to overtop the device as it passed (Figure 13). The overtopping did not occur when the flap was near-vertical and had a significant effect on the time-resolved dynamics. We are currently investigating how these dynamics change with and without overtopping and if there are conclusions we can draw from the data to explain the physics of this phenomenon.

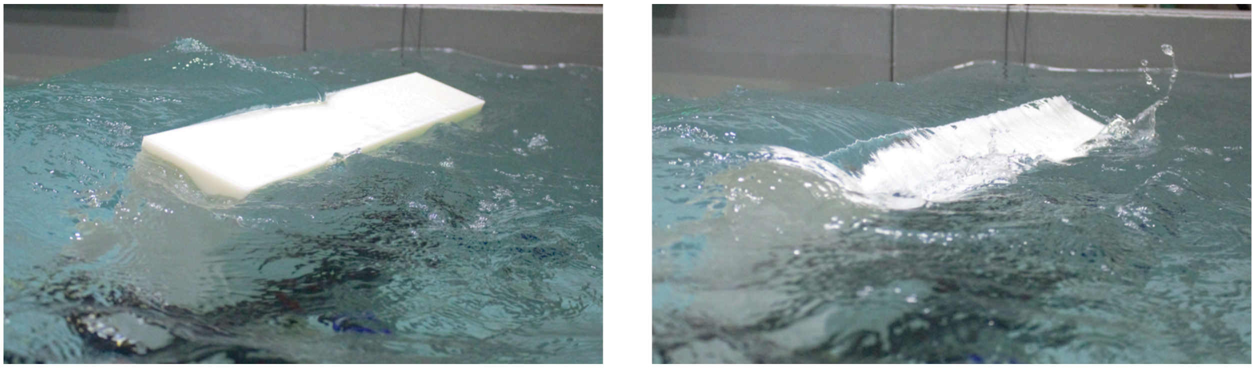

Figure 13: An example of the square flap before (left) and during (right) an overtopping event. These images were taken during a PTO damping sweep test.

The second observation is that confinement plays a significant role in the dynamics, particularly at certain wave and oscillation frequencies. Specifically, we observed standing waves in the cross-tank direction perpendicular to the incident wave during tests. The magnitude of these standing waves varied with wave frequency, as certain wavelengths resulted in constructive interference for the cross-tank waves. Specifically, waves with a period between a 1.2 and 1.3 seconds, corresponding to a wavelength between 2.3 and 2.6 meters, resulted in the largest magnitude standing waves due to resonance in the 2.5 meter wide tank. We expect these waves are a consequence of the reflection of radiated and/or diffracted waves that have a component in the cross-tank direction. An example of these waves is shown in Figure 14. Over time throughout the test, the reflections sometimes resulted in a sharp wave peak that occurred in the center of the flap (Figure 14). This caused some overtopping near the center of the flap and changes in the span-wise wave elevation on the flap face.

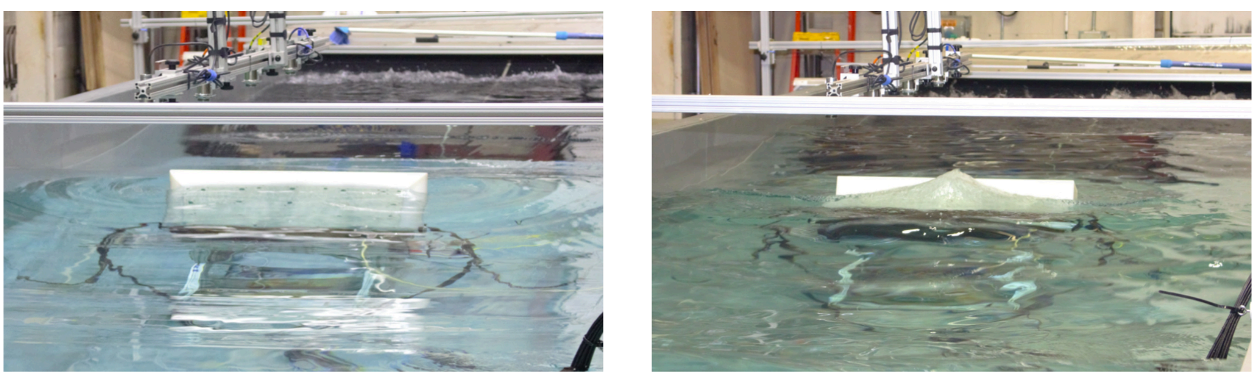

Figure 14: [Left] Example of wave patterns around the flap during testing. [Right] Example of a wave peak in the center of the flap due to standing waves caused by the reflection from the tank walls.

7.2 Lesson Learned and Test Plan Deviation

Lessons Learned: There were a significant number of lessons learned during this project, including:

- *Data collection*: Viewing data in real time was instrumental in changing and debugging our controller, which allowed us to complete the tests in the time allotted. The range of data we were able to rapidly visualize also helped ensure that the device was working properly throughout the experimental campaign.

- *Testing procedures*: Checklists for different testing procedures were extremely helpful to ensure we did not skip steps that could damage equipment. We made checklists for installing and removing the OSWEC from the tank, starting up and shutting down the wavemaker, and starting and managing the controller.

- *Flexibility in test plan and setup*: Although planning the test plan and setup was a critical step to completing these experiments, there were inevitable adjustments we needed to make to our system and test plan as we learned from the initial tests. This included adjusting cable routing to avoid biasing performance measurements and adjusting the test plan to account for hardware limitations. This flexibility was essential to completing the test with high-value, publishable data.

- *Stiction*: During the PTO damping tests, we discovered that the stiction in the driveline was a significant fraction of the torque applied to the flap, particularly for tests with smaller wave heights (e.g., 50 mm). Because of this, we needed to update our definition of PTO damping to include the effect of these losses, particularly since they acted in phase with velocity. This motivated us to define the effective damping parameter, $B_{PTO,eff}$ (Section 6.6.3) to account for these losses. This also led to adding stiction compensation tests, which helped us mitigate and understand the effect of stiction altogether (Figure 12).

- *Logistics*: The two main differences between tests that had previously been conducted with this test article at UW and test at NREL were (1) elevated Health & Safety requirements for electrical protection around water and (2) an inability to drain the tank during OSWEC installation and removal. The first was the subject of multiple discussions between the UW and NREL teams ahead of the tests and resulted in an overall safer system that passed Health & Safety inspection without difficulty. At the same time, meeting these requirements involved a significant and unanticipated effort for the UW team, both in terms of personnel time and materials for equipment modification. Second, because NREL does not have a municipal water connection or holding basin, it is not feasible to decrease tank water levels or empty the tank entirely for installation. In addition, Health & Safety requirements restrict personnel entry to the tank. Consequently, a new test procedure was required to lift the OSWEC in and out of the tank in a fully assembled state. We tested this procedure at UW, but did not anticipate the NREL requirement for a certification on the spreader bar used for lifting. We were able to navigate this challenge, but recommend that future tests discuss certification requirements for lifts around SWEL.

Test Plan Deviation: There were a number of deviations we made from the original Test Plan, including:

- *Buoyancy tests*: We added tests to characterize the buoyancy as a function of flap position. This information was needed to isolate added inertia and radiation damping in the forced oscillation data analysis, emulate additional buoyancy, and for future modeling efforts. These tests were not included in the original test plan because we had planned on a different method for estimating weight and buoyancy torques. However, because we were operating at a single water depth for these tests, we realized we could significantly simplify our methods and increase the accuracy of our buoyancy torque estimates.

- *Excitation tests*: We did not run some of the planned excitation tests due to unanticipated limitations on the wavemaker. These are now better understood by NREL and can be communicated ahead of future testing in SWEL.

- *Forced oscillation tests*: We had to significantly decrease the oscillation amplitudes tested to avoid exceeding the motor torque limit and the calibrated region for the load cells. We were not able to anticipate this in advance because the full range of oscillation amplitudes and periods had not been tested at UW in advance of shipping the OSWEC to NREL. However, the revised approach minimally affected the overall project objectives.

- *Control tests*: The largest deviation we made to the test plan was shifting away from data-driven MPC to instead address experimental artifacts including low flap buoyancy and stiction. There were three issues involved in this deviation. First, the MPC controller was not ready for testing when we arrived at NREL due to prioritizing hardware readiness. In addition, we found that it was difficult to ensure stability and accuracy of DMD for real-time control, even in a simplified testing environment such as WEC-Sim. Thus, controller testing in hardware could have unexpectedly exceeded load cell or motor limits, compromising the test article. Second, the irregular waves that could be generated in SWEL resulted in limited flap motion, such that MPC testing would not have been representative of real-world conditions. Third, flap motion in irregular seas was limited, in part, by the relatively low flap buoyancy and relatively high driveline stiction. The latter meant that a substantial fraction of the applied torque would be uncontrollable. By shifting focus to understanding and compensating for these scale-model artifacts we were able to investigate the underlying dynamics of the device in relation to control and power performance. Because of this, these unanticipated tests were essential to understanding the OSWEC sufficiently to inform future control research.

- *Flap profiles*: Because water depth could not be adjusted, instead of running tests at two different submergence depths, we instead tested two different flap profiles: one with round and one with square edges. We did this so we could potentially investigate BEM accuracy for different flap edges, which we expect to have a significant effect on drag and viscous losses. This change had minimal effect on the test plan and was a change informed by observed performance and questions formed during testing.

- *Scheduling*: We initially planned for tests to occur in a five week period. Instead, we tested for a total of ten weeks, with a four month break after the seventh week. During this break in testing, we analyzed the data in detail to ensure its quality, and also updated the test plan for the final three weeks to account for gaps in the data set based on our research questions. Although both the time we were testing and the time required to run the analysis was longer than anticipated, the extra time was needed to understand the data we had collected and feel confident we would collect all the data needed for anticipated publications. To avoid this type of delay in the future, we would recommend allocating even more time for debugging and data analysis when test articles have had limited use.

8 Conclusions and Recommendations

During this project, we successfully characterized the buoyancy torque as a cubic function of position for both the round and square flaps. We then extracted excitation torque coefficients from locked flap tests and demonstrated strong agreement with BEM, especially when including channel walls in simulation. Next, we extracted added inertia and radiation damping as a function of oscillation period from the forced oscillation tests for both the round and square flaps. For both edge profiles, experimental values of added inertia were consistently lower than BEM for periods less than 1.4 seconds, but agreed well for periods above 1.4 seconds. For radiation damping, the experimental values for the both flaps were consistently greater than those predicted from BEM, especially near the cross-channel resonant period of 1.25 seconds. We expect this to be due to viscous and confinement effects not captured by BEM, even when including channel walls. These deviations were more prominent for the square flap, which is consistent with increased viscous losses from the sharp edges. Overall, we found that agreement between BEM and experiments varied for different hydrodynamic parameters and disagreement can arise from several sources including confinement, viscous, and surface effects. In addition, adding a channel to BEM simulations improved agreement with experimental excitation torque coefficients, but did not substantially improve agreement with experiments for radiation damping and added inertia coefficients. This suggests that care should be taken when using BEM with or without explicitly modeling channel walls, even when a model is about ⅓ of the channel width. The extent to which the disagreements between BEM and experiments observed here represent fundamental limits to BEM (e.g., neglecting viscous losses) versus conditions unique to these experiments (e.g., confinement effects) requires further study. Finally, we investigated the performance of both flaps under linear damping control for a range of wave and flap properties. We found that flap performance was highly dependent on wave period and height, with a period of 1.5 seconds being the best-performing wave period tested. We also identified that increased flap buoyancy can increase CWR and reduce the effective damping coefficient where the max CWR occurs. Further, we found that the flap shape significantly affects performance, but only at higher damping values and that changes in buoyancy had a smaller effect on CWR for the square flap, particularly for lower effective damping values. Lastly, we were successful in applying a control torque to counteract the stiction present in the driveline. With these results, we were successful in our goal of investigating the system to inform future control research. Although we shifted from our initial plan of employing a data-driven model predictive controller to optimize flap performance, we were able to understand and compensate for experimental artifacts that affect flap dynamics and control. Overall, these results show the importance of experimental testing to understand trends in device dynamics and performance.

Using this data set, UW plans to further investigate the time-resolved dynamics to identify properties of the dynamics that explain these results. We also plan to use this data set to inform data-driven modeling efforts, with specific interest in identifying and characterizing artifacts of nonlinearity. We also plan to further investigate the effect of confinement and flap edge on hydrodynamic parameters when compared to BEM.

Data used in this work is available on the MHK DR under the title “Experimental Characterization of a Laboratory-Scaled Oscillating Surge Wave Energy Converter”.

9 References

[1] C. Lee and J. Newman, “WAMIT User Manual,” 2006, Available: https://www.wamit.com/manual.htm

[2] Crooks, David, et al. "Oscillating wave surge converter forced oscillation tests." *International Conference on Offshore Mechanics and Arctic Engineering*. Vol. 49972. American Society of Mechanical Engineers, 2016.

[3] McIver, P., and D. V. Evans. "The occurrence of negative added mass in free-surface problems involving submerged oscillating bodies." *Journal of engineering mathematics* 18.1 (1984): 7-22.

10 Acknowledgements

We would like to thank Rebecca Fao and Mike Lawson for their help organizing and planning this project at NREL. We thank Charles Candon, Mark Murphy, Kyle Swartz, and Victor Castillo for their assistance working with the OSWEC and the wave tank at NREL. We would also like to thank Harlin Wood, Corey Crisp, Greg Talpey, and Gemma Calandra for their help developing the hardware and software with the project from UW. Finally, we thank Ama Hartman for leading the development of the OSWEC device and for her assistance running experiments at NREL.

11 Appendix

11.1 DAQ Specifications

Table 11.1.1: Details on DAQ system.

Channel	Measured physical quantity	Engineering units	Measurement type	Data rate	Range of measurement
68	Load Cell 1: Gage 1+	Volts	Analog	1000 Hz	±10 V
34	Load Cell 1: Gage 1-	Volts	Analog	1000 Hz	±10 V
33	Load Cell 1: Gage 2+	Volts	Analog	1000 Hz	±10 V
66	Load Cell 1: Gage 2-	Volts	Analog	1000 Hz	±10 V
65	Load Cell 1: Gage 3+	Volts	Analog	1000 Hz	±10 V
31	Load Cell 1: Gage 3-	Volts	Analog	1000 Hz	±10 V
64	Load Cell 1: Ground (Cable shield)	Volts	Analog	1000 Hz	±10 V
30	Load Cell 1: Gage 4+	Volts	Analog	1000 Hz	±10 V
63	Load Cell 1: Gage 4-	Volts	Analog	1000 Hz	±10 V
28	Load Cell 1: Gage 5+	Volts	Analog	1000 Hz	±10 V

TEAMER
Testing & Expertise for Marine Energy

61	Load Cell 1: Gage 5-	Volts	Analog	1000 Hz	±10 V
60	Load Cell 1: Gage 6+	Volts	Analog	1000 Hz	±10 V
26	Load Cell 1: Gage 6-	Volts	Analog	1000 Hz	±10 V
22	Motor drive control	Volts	Analog	1000 Hz	±10 V
55	Motor drive control	Volts	Analog	1000 Hz	±10 V
51	Relays: Signal	Volts	Digital	1000 Hz	5 V
17	Relays: Signal	Volts	Digital	1000 Hz	5 V
50	Relays: Signal	Volts	Digital	1000 Hz	5 V
16	Relays: Signal	Volts	Digital	1000 Hz	5 V
49	Relays: Signal	Volts	Digital	1000 Hz	5 V
14	Relays: Power Leak detector: Power Limit switch: Power	Volts	Digital	1000 Hz	5 V
52	Limit switch: Signal	Volts	Digital	1000 Hz	5 V
15	Leak detector: Signal	Volts	Digital	1000 Hz	5 V
48	Leak detector: Signal	Volts	Digital	1000 Hz	5 V
3	Encoder 1: Signal	Counts	Digital	1000 Hz	5 V
37	Encoder 1: Signal	Counts	Digital	1000 Hz	5 V
45	Encoder 1: Signal	Counts	Digital	1000 Hz	5 V
8	Encoder 1: Power Encoder 2: Power	Volts	Digital	1000 Hz	5 V
46	Encoder 2: Signal	Counts	Digital	1000 Hz	5 V
42	Encoder 2: Signal	Counts	Digital	1000 Hz	5 V
41	Encoder 2: Signal	Counts	Digital	1000 Hz	5 V
7	Encoder 1: Ground Encoder 2: Ground	Volts	Digital	1000 Hz	5 V
68	Load Cell 2: Gage 1+	Volts	Analog	1000 Hz	±10 V
34	Load Cell 2: Gage 1-	Volts	Analog	1000 Hz	±10 V
33	Load Cell 2: Gage 2+	Volts	Analog	1000 Hz	±10 V
67	Load Cell 2: Gage 2-	Volts	Analog	1000 Hz	±10 V
66	Load Cell 2: Gage 3-	Volts	Analog	1000 Hz	±10 V
32	Load Cell 2: Gage 3+	Volts	Analog	1000 Hz	±10 V
65	Load Cell 2: Gage 4+	Volts	Analog	1000 Hz	±10 V

31	Load Cell 2: Gage 4-	Volts	Analog	1000 Hz	±10 V
64	Load Cell 2: Gage 5-	Volts	Analog	1000 Hz	±10 V
30	Load Cell 2: Gage 5+	Volts	Analog	1000 Hz	±10 V
63	Load Cell 2: Gage 6-	Volts	Analog	1000 Hz	±10 V
29	Load Cell 2: Gage 6+	Volts	Analog	1000 Hz	±10 V
22	Load cell 2: Ground	Volts	Analog	1000 Hz	±10 V